COMMUNICATION

Reduced graphene oxide–silicon interface involving direct Si–O bonding as a conductive and mechanical stable ohmic contact

Soraya Rahpeima,[ab] Essam M. Dief,[a] Chandramalika R.Peiris,[a] Stuart Ferrie,[a] Alex Duan,[c] Simone Ciampi,[a] Colin L. Raston[*b] and Nadim Darwish[*a]

Received 00th January 20xx,
Accepted 00th January 20xx

DOI: 10.1039/x0xx00000x

Metal–semiconductor junctions are essential contacts for semiconductor devices, but high contact junction resistance is a limiting operational factor. Here, we establish an ohmic contact of low resistance of < 4 × 10^{-6} Ωcm² between platinum and n-type Si (111)–H surfaces. This involved Si–O covalent bonding a monolayer of graphene oxide (GO) to the Si surface followed by electrochemical reduction to form reduced graphene oxide (rGO). Current–voltage plots demonstrate that the GO/rGO transformation is associated with a change from a rectifying to an ohmic contact. The process is a viable method for constructing semiconductor–rGO interfaces and demonstrates that GO/rGO monolayers can be used as active components in tuning the contact resistance of metal–semiconductor junctions.

Metal−semiconductor (M−S) junctions are key elements for many technologies including Si−based devices.[1-8] For instance, M−S interfaces govern the switching speed in diodes, the on-state and off-state currents in transistors, and the open circuit voltage in solar cells.[9] When a metal forms a contact with a semiconductor, a potential barrier – a Schottky barrier is usually formed due to the misalignment between the metal work function and the electron or hole affinity of the semiconductor. The Schottky barrier causes high contact resistance at the junction but semiconducting devices, or more generally integrated circuits, require ohmic contacts with other electronic systems for proper device operations. For example, an ohmic contact can enable charge conduction between the active region of transistors and the external circuitry.[10] In principle, metals should form ohmic contacts without any Schottky barriers if their work functions aligns with the conduction or valence band edges of semiconductors. In practice, however, metals form Schottky contacts irrespective of work function since the Fermi-level of a metal is pinned at a certain energy level at the semiconductor interface. This makes it difficult to fabricate ohmic contacts or even Schottky diodes with barrier heights predicted from work functions differences only. Such Fermi-level pinning has been attributed to surface states, formation of defects at the interface and the existence of lattice distortion, and are common for semiconductors such as Si and GaAs.[11, 12]

Low contact resistance of metals to Si has been achieved but not without limitations. For instance, incorporating highly doped semiconductors have been shown to reduce the contact resistance by reducing the barrier width as an alternative option to reducing the barrier height. However, this approach introduces difficulties in controlling the dopant profile when the size of the device reaches the nanoscale regime.[13] Another approach involves de-pinning of the Fermi-level, i.e. reducing the barrier height, by inserting an interfacial layer between the parent metal and Si.[14, 15] The inter-layer functions as a passivating layer to reduce the defects at the metal–Si interface while being conductive enough for significant charge carrier transport through it. The latter approach is nevertheless technically challenging in maintaining interfacial uniformity and mechanical stability across the M−S junction. Other methods involve the physical insertion of insulating films such as SiN, TiO_2, or ZnO. The inserted insulator lowers Fermi-level pinning; however, the insulating barrier decreases the tunneling current through the barrier, therefore impedes reduction of the contact resistance. [16-18] Recently, an ohmic junction was constructed, by physically inserting a graphene or boron nitride layer between the metal and n-type Si.[19, 20] The interfacial 2D material has two roles, in preventing Fermi-level pinning and modulating the work function to align with the conduction band edges of the semiconductor.[19, 20]

We have developed an ohmic contact between Si and platinum electrodes by covalently attaching a monolayer of reduced graphene oxide (rGO) to the H−terminated Si (Si−H) electrode. This takes advantage of the recently reported spontaneous Si−O linkages via OH groups reacting with freshly prepared Si−H surfaces.[21] Following this reaction, an electrochemical reduction was performed to convert the GO to rGO. The constructs were then extensively characterised using atomic force microscopy (AFM), X-ray photoelectron spectroscopy (XPS) and cyclic voltammetry (CV) for determining topography, surface composition, and electron transfer properties. The ohmic contact was tested by means of conducting atomic force microscopy using a platinum AFM tip and by recording current–voltage characteristics of the Pt–GO–Si and Pt–rGO–Si junctions.

[a] School of Molecular and Life Sciences, Curtin Institute of Functional Molecules and Interfaces, Curtin University, Bentley, WA 6102, Australia. Email: nadim.darwish@curtin.edu.au
[b] Flinders Institute for Nanoscale Science and Technology, College of Science and Engineering, Flinders University, Adelaide, SA 5001, Australia. Email: colin.raston@flinders.edu.au
[c] Trace Analysis for Chemical, Earth and Environmental Sciences (TrACEES), The University of Melbourne, Melbourne, VIC 3010, Australia
Electronic Supplementary Information (ESI) available: [details of any supplementary information available should be included here]. See DOI: 10.1039/x0xx00000x

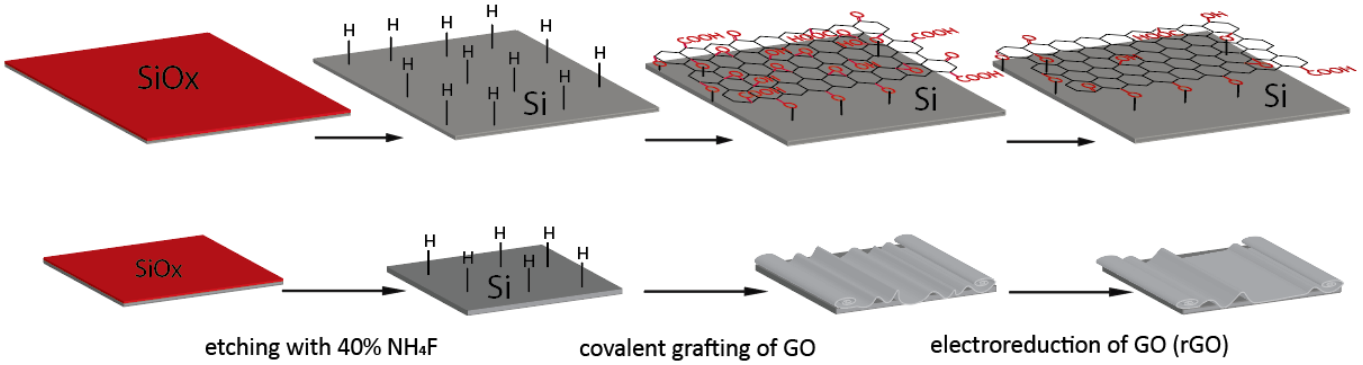

Scheme1. Schematic describing the fabrication procedure: Si wafer with native oxide is etched in aqueous NH_4F to form Si–H surfaces which were then incubated in 2 mg mL^{-1} of GO for 24 h to covalently attach the GO layer via Si–O bonds followed by electrochemically reduction of the GO layer to rGO.

Covalently attaching GO to Si simply involves immersing a freshly prepared Si–H electrode in 2 mg mL^{-1} aqueous suspension of GO (Scheme 1). Fig. 1(a) shows the AFM topography image of GO modified Si–H n-type (111) surface. A key finding here is the presence of an ultra-thin layer of GO that is hardly visible under SEM or AFM microscopy. Indeed, the presence of such a thin layer of GO is inferred from observing some folded and wrinkled areas which have higher thicknesses and appear brighter in AFM topography images. Another key finding is that the GO sheets follow the topography of the Si–H (111) terraces. This is particularly important as the GO forms a uniform layer and protects the highly reactive Si–H surface from further reactions.

The GO–Si surface was then electrochemically reduced to rGO through multiple reduction cycles. Fig. 1(b) shows the cyclic voltammograms of the reduction of the GO–Si surface at a scan rate of 50mV s^{-1}. A broad GO reduction wave was observed at −965 mV vs Ag/AgCl for GO–Si surface while there are no voltametric waves for a bare Si–H surface, as shown in inset of Fig. 1(b). This confirms that the wave at −965 mV corresponds to the reduction of the GO layer. In the second reduction cycle, the reduction wave diminishes by ~ 75 %. Further potential cycling leads to further diminishing in the reduction wave with a concomitant shift towards negative potentials. After 10 cycles the reduction peak is 5-10 % from that of the initial peak. This was observed for most scan rates (see Fig. S1 of the Electronic Supplementary Information (ESI). We speculate that the first reduction peak corresponds to the reduction of the oxygen species on the flat areas of the Si–GO junctions while the proceeding reduction waves correspond to the reduction of the oxygen species in the partially scrolled and wrinkled areas (Fig. S3, ESI) which require higher cathodic potentials for the reduction.

AFM topography images after electrochemical reduction of GO are shown in Fig. 1(c). The rGO sheets remain attached to the surface of the electrode despite 10 potential cycles between −1500 and +200 mV. We emphasise here that the presence of a thin layer of reduced graphene oxide is inferred from the presence of wrinkles and partial scrolls at certain areas while the flat areas are those following uniformly the Si (111) terraces analogous to a carpet on stairs, Fig. 1(d). Despite some areas which showed wrinkled GO/rGO layers (Fig. S3), AFM topography images largely show that silicon terraces are visible underneath the GO layers (without white spots), indicating the protection of the silicon against oxidation by the GO bonding (Fig. S5, ESI).

XPS show that the ratio of C–C vs other C–O/C=O/COO is 3:2 vs 3:1 for the Si–GO vs Si–rGO, respectively, Fig. 2. This is attributed to the reduction of the oxygen content by the electrochemical reduction which consequently enhances the C–C content over the other C–O species.

The reduction in the oxygen species can also be inferred from the C/O ratio which is 1.2 versus 2.1 for the Si–GO and the Si–rGO, respectively (see Fig. S6, ESI). The peaks in the binding energy range of 102–104 eV are assigned as arising from Si–O–C for Si–GO and Si–rGO, respectively. The assignment of peak for Si–O–C rather than Si–Ox is supported by (a) no reaction between a pre-oxidized Si-Ox surface and GO (see Fig. S7, ESI), and (b) XPS of a Si-H surface incubated in water for 24 h showed negligible Si-Ox signals (Fig. S9, ESI) and (c) ferrocene methanol (a molecule that has OH groups as in GO) forms Si-O-C bonds as demonstrated by electrochemistry and XPS (Fig. S8, ESI). Moreover, all our AFM images clearly show Si (111) terraces underneath the GO and the rGO layers with limited white spots (oxide) – an observation that is not possible if large quantities of SiOx is present on the surface.

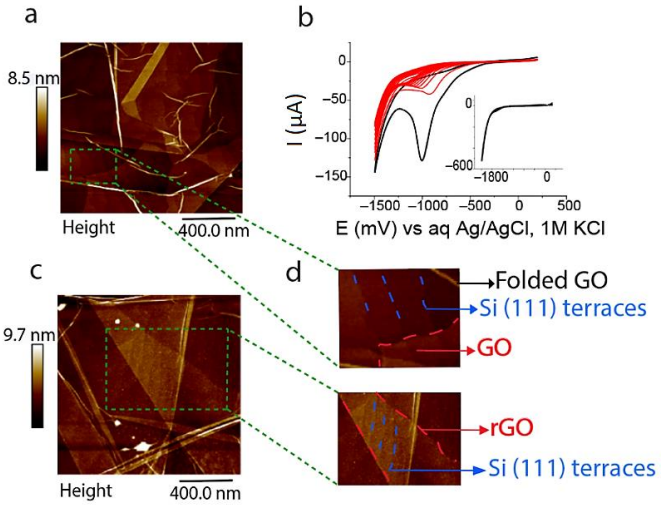

Fig1. (a) AFM topography image of the covalent bound GO on the Si–H (111) (Si–GO). (b) 10 consecutive cycles of cyclic voltammetry for the electrochemical reduction of GO in 0.1 M phosphate buffer solution at a pH 7.4 and a scan rate of 50 mV s^{-1}. The inset in (b) depicts the cyclic voltammetry response of the Si–H (111) in the same buffered solution and scan rate. (c) AFM topography image of rGO modified Si–H (111) (Si–rGO). (d) Zoomed-in areas of the Si–GO and Si–rGO showing monolayers of GO and rGO covering Si (111) terraces that are separated by atomic steps. See Fig. S2 and Fig. S4, ESI for detailed AFM analysis.

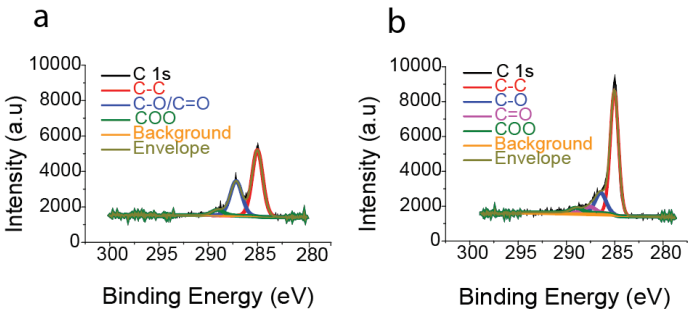

Fig. 2. Carbon high resolution scans of GO-Si (a) and rGO-Si (b). The ratio of C–C vs other C–O/C=O/COO is 3:2 vs 3:1 for the Si–GO vs Si–rGO, respectively. Survey and silicon high resolution scans of Si–GO and Si–rGO are presented in Fig. S6, ESI.

The AFM and XPS data is consistent with the GO/rGO layer protecting the Si substrate from ambient oxidation, by forming a monolayer of Si–GO and Si–rGO. This is a significant finding for practical modification of Si surfaces.

Current-voltage (I–V) measurements of the Si–H–Pt, Si–GO–Pt and Si–rGO–Pt junctions are shown in Fig. 3. Key observations are (a) when the intervening layer between the Pt and the Si electrode is GO (*i.e.* Si–GO–Pt) there is limited change in the reverse current while there is significant decrease in the forward current, and (b) the (I–V) characteristics change from a current rectifier in Fig. 3(a) and Fig. 3(b) to ohmic after electrochemical reduction of GO, Fig. 3(c). This can be explained as follows, that the difference in the work function between platinum and Si (~ 1 eV) and the Fermi level pinning leads to the expected current rectification observed in Fig. 3(a). When GO separates platinum and the Si electrode (Si–GO–Pt), the forward current is reduced due to the insulating property of the GO layer. However, when rGO forms the interfacial layer (Si–rGO–Pt), the contact change from being a rectifier to ohmic, due to the Fermi-level depininng introduced by the Si–O connected rGO layer which forms dipoles at the interface. As a result, an electrical potential drop is built up at the interface which should be added to the energy bend bending which effectively reduces the barrier height (Fig. 4). Hence, the Pt–rGO junction shifts the pinning point toward the Si conduction band, decreasing the Schottky barrier height (Fig. 4b). We stress here that the interfacial 2D material must be highly conducting as the change in the contact resistance was only observed when rGO was the interfacial material while the opposite, *i.e.* higher resistance, was observed when GO forms the interfacial layer.

Fig. S13 of the ESI show current–voltage measurements for the Si–GO surface that is reduced by different number of electrochemical reduction cycles which alters the GO/rGO ratios. The corresponding I-V curves show that the current increases with the increase in the reduction cycles from 1 to 5. After 5 reduction cycles, there is no change in the ohmic I-V curves, indicating the highest percentage of rGO has been reached. This indicate that electrochemical gating can be used to further tune the I-V properties of the Si–GO/rGO junction.

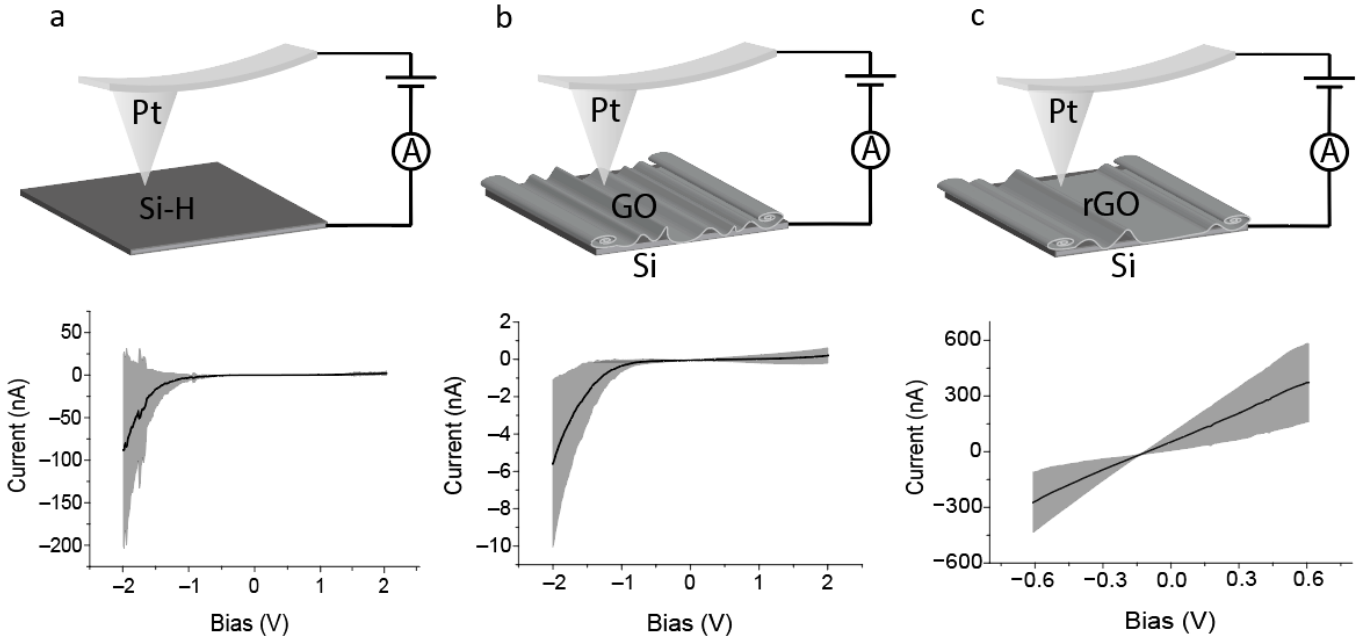

Fig 3. Schematics and AFM current–voltage (I–V) measurements with solid lines representing the average of 20 different (I–V) plots of (a) Si–H–Pt, (b) Si–GO–Pt, and (c) Si–rGO–Pt junctions. The bias is applied to the Si surface, with bias sweep set between –2 and +2 V for (a) and (b) and – 0.6 V to + 0.6 V for (c) given that beyond these values, the current amplifier of the C-AFM system is saturated (see Fig. S12, ESI). The (I–V) characteristics switch from being a rectifier in (a) and (b) to ohmic after the electrochemical reduction of GO in (c). The contact resistance in (c) is calculated from the slope of the averaged I–V plots.

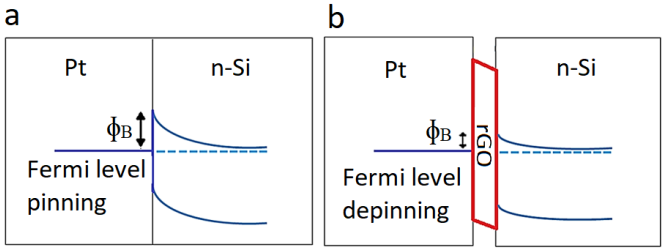

Fig 4. Schematic band diagrams in the absence (a) and presence (b) of the rGO interfacial layer. The contact is a rectifier in (a) due to a pinned Fermi level near the conduction band. The contact changes from being a rectifier to ohmic in (b) due to the Fermi-level depininng introduced by the Si–O connected rGO dipole and the high conductivity of the rGO layer. The Pt–rGO junction shifts the pinning point toward the Si conduction band, thereby decreasing the height of the Schottky barrier (ϕ_B).

In summary, we have developed a simple chemical method for covalently attaching GO/rGO to Si electrodes, involving Si–O linkages. The GO/rGO layer follows the topography of the Si (111) terraces and protects the Si substrate from oxidative damage with the bound GO monolayer electrochemically reduced to rGO without desorption from the Si surface. The covalent bonding is spontaneous and requires no heating, UV irradiation or external catalysis. This enabled mechanically robust and low resistive Pt/rGO/n-type Si contacts which are otherwise highly resistive and rectifying without the rGO interfacial layer. Current–voltage measurements of the Pt/GO/rGO/n-type Si contacts showed switching from a rectifying to a low-resistance ohmic contact < 4×10^{-6} Ωcm^2, when GO is reduced to rGO between the Pt and the Si electrodes – a phenomenon that is explained by Fermi level depinning introduced by the Si–rGO bonding upon the electrochemical reduction of GO. The methodology developed herein will contribute to the high-resistive contact issue commonly encountered in semiconductor technologies and opens new avenues for incorporating 2D materials in miniaturised electronics.

The authors would like to acknowledge the Australian Research Council (DP190100735, DE160101101 and DE160100732, DP170100450) for funding and Microscopy Australia for support of this work.

Conflicts of interest

There are no conflicts to declare.

Notes and references

1. A. C. Aragonès, N. Darwish, S. Ciampi, F. Sanz, J. J. Gooding and I. Díez-Pérez, *Nat. Commun.*, 2017, 8, 1-8.
2. C. R. Peiris, Y. B. Vogel, A. P. Le Brun, A. C. Aragonès, M. L. Coote, I. Díez-Pérez, S. Ciampi and N. Darwish, *J. Am. Chem. Soc.*, 2019, 141, 14788-14797.
3. A. Vezzoli, R. J. Brooke, N. Ferri, C. Brooke, S. J. Higgins, W. Schwarzacher and R. J. Nichols, *Faraday Discuss.*, 2018, 210, 397-408.
4. A. Vezzoli, R. J. Brooke, N. Ferri, S. J. Higgins, W. Schwarzacher and R. J. Nichols, *Nano lett*, 2017, 17, 1109-1115.
5. A. Vezzoli, R. J. Brooke, S. J. Higgins, W. Schwarzacher and R. J. Nichols, *Nano lett*, 2017, 17, 6702-6707.
6. Y. B. Vogel, L. Zhang, N. Darwish, V. R. Gonçales, A. Le Brun, J. J. Gooding, A. Molina, G. G. Wallace, M. L. Coote and J. Gonzalez, *Nat. Commun.*, 2017, 8, 1-9.
7. Y. Xu, C. Cheng, S. Du, J. Yang, B. Yu, J. Luo, W. Yin, E. Li, S. Dong and P. Ye, *ACS nano*, 2016, 10, 4895-4919.
8. L. Zhu, R. T. Popoff and H.-Z. Yu, *J. Phys. Chem. C*, 2015, 119, 1826-1831.
9. R. Chang, S. Asatyas, G. Lkhamsuren, M. Hirohara, E. A. Q. Mondarte, K. Suthiwanich, T. Sekine and T. Hayashi, *Polym. J.*, 2018, 50, 563-571.
10. L. M. Porter, K. Das, Y. Dong, J. H. Melby and A. R. Virshup, in *Comprehensive Semiconductor Science and Technology*, eds. P. Bhattacharya, R. Fornari and H. Kamimura, Elsevier, Amsterdam, 2011, pp. 44-85.
11. E. H. Rhoderick, *IEE Proc.-I: Solid-State Electron Devices*, 1982, 129, 1.
12. H. J. Lewerenz, *J. Electroanal. Chem.*, 1993, 356, 121-143.
13. Y. Wan, C. Samundsett, J. Bullock, M. Hettick, T. Allen, D. Yan, J. Peng, Y. Wu, J. Cui, A. Javey and A. Cuevas, *Adv. Energy Mater.*, 2017, 7, 1601863.
14. D. Connelly, C. Faulkner, P. A. Clifton and D. E. Grupp, *Appl. Phys. Lett.*, 2006, 88, 012105.
15. S. Zheng, H. Lu, H. Liu, D. Liu and J. Robertson, *Nanoscale*, 2019, 11, 4811-4821.
16. A. Agrawal, J. Lin, B. Zheng, S. Sharma, S. Chopra, K. Wang, A. Gelatos, S. Mohney and S. Datta, 2013 Symp. VLSI Technol, 2013, T200-T201.
17. J. Hu, A. Nainani, Y. Sun, K. C. Saraswat and H.-S. Philip Wong, *Appl. Phys. Lett.*, 2011, 99, 252104.
18. P. Paramahans, S. Gupta, R. Mishra, N. Agarwal, A. Nainani, Y. Huang, M. Abraham, S. Kapadia, U. Ganguly and S. Lodha, *Symp. VLSI Technol.*, 2012, 83-84.
19. K.-E. Byun, H.-J. Chung, J. Lee, H. Yang, H. J. Song, J. Heo, D. H. Seo, S. Park, S. W. Hwang, I. Yoo and K. Kim, *Nano Lett.*, 2013, 13, 4001-4005.
20. M.-H. Lee, Y. Cho, K.-E. Byun, K. W. Shin, S.-G. Nam, C. Kim, H. Kim, S.-A. Han, S.-W. Kim, H.-J. Shin and S. Park, *Nano Lett.*, 2018, 18, 4878-4884.
21. J. Escorihuela and H. Zuilhof, *J. Am. Chem. Soc.*, 2017, 139, 5870-5876.

